Structural Characterization of Three Crystalline Modifications of Telmisartan by Single Crystal and High-Resolution X-ray Powder Diffraction

ROBERT E. DINNEBIER,[1] PETER SIEGER,[2] HERBERT NAR,[2] KENNETH SHANKLAND,[3] WILLIAM I. F. DAVID[3]

[1] Laboratory of Crystallography, University of Bayreuth, D-95440, Bayreuth, Germany

[2] Departments of Analytical Sciences and Medicinal Chemistry, Boehringer Ingelheim Pharma KG, D-88397 Biberach a.d. Riss, Germany

[3] ISIS Facility, Rutherford Appleton Laboratory, Chilton, Didcot, Oxon, United Kingdom OX11 0QX

Received 14 March 2000; revised 25 July 2000; accepted 2 August 2000

ABSTRACT: Three crystalline modifications (A, B, and C) of 4′-[[2-*n*-propyl-4-methyl-6-(1-methyl-benzimidazol-2-yl)benzi midazol-1-yl]methyl]biphenyl-2-carboxylic acid (INN name, telmisartan) have been detected and their crystal structures have been determined by single-crystal X-ray diffraction (pseudopolymorph C) and the method of simulated annealing from high-resolution X-ray powder diffraction data (polymorphs A and B). The compound is of interest because of its use as an angiotensin II receptor antagonist. Polymorph A crystallizes in space group $P2_1/c$, $Z = 4$, with unit cell parameters $a = 18.7798(3)$, $b = 18.1043(2)$, and $c = 8.00578(7)$ Å, $\beta = 97.066(1)°$, and $V = 2701.31$ Å^3. Polymorph B crystallizes in space group $P2_1/a$, $Z = 4$, with unit cell parameters $a = 16.0646(5)$, $b = 13.0909(3)$, and $c = 13.3231(3)$ Å, $\beta = 99.402(1)°$, and $V = 2764.2(1)$ Å^3. The solvated form C crystallizes in space group $C2/c$, $Z = 8$, with unit cell parameters $a = 30.990(5)$, $b = 13.130(3)$, and $c = 16.381(3)$ Å, $\beta = 95.02(2)°$, and $V = 6639(2)$ Å^3. For the structure solutions of polymorphs A and B, 13 degrees of freedom (3 translational, 3 orientational, 7 torsion angles) were determined in ~2 h of computer time, demonstrating that the crystal packing and the molecular conformation of medium-sized (MW ≈ 500) pharmaceutical compounds can now be solved quickly and routinely from high-resolution X-ray powder diffraction data. J Pharm Sci 89: 1465–1479, 2000

Keywords: powder diffraction; polymorphism; simulated annealing; telmisartan; angiotensin II receptor antagonist

INTRODUCTION

The tendency for pharmaceutical solids to crystallize in multiple crystal forms and the significance of this phenomenon (polymorphism) have been demonstrated.[1,2] Because polymorphism can affect the chemical, biological, and pharmaceutical properties of the drug, it is very important to detect polymorphic, solvated, or amorphous forms of the drug substance. In this study, the different polymorphic forms of the drug substance telmisartan (4′-[[2-*n*-propyl-4-methyl-6-(1-methylbenzimidazol-2-yl)benzimidazol-1-yl]methyl]biphenyl-2-carboxylic acid) are investigated.

Telmisartan is a new, orally active, nonpeptide angiotensin II receptor antagonist. The renin–angiotensin system (RAS) plays an important role in the control of blood pressure[3] and the regulation of volume and electrolyte homeostasis.[4] The therapeutic success of the angiotensin-converting

Correspondence to: R. E. Dinnebier (Telephone: 0049 921 553880; Fax: 0049 921 553770; E-mail: robert.dinnebier@uni-bayreuth.de)

Journal of Pharmaceutical Sciences, Vol. 89, 1465–1479 (2000)

enzyme inhibitors has demonstrated the advantage of pharmacological interference with the RAS in hypertension and congestive heart failure. This result stimulated the search for additional pharmacological interventions with the RAS; namely, renin inhibitors and angiotensin II receptor antagonists. The drug substance Telmisartan is a potent representative of the latter.

Telmisartan is a novel substituted benzimidazole derivative (see Figure 1). The complete synthesis and the proof of the molecular structure [by ^{1}H and ^{13}C, nuclear magnetic resonance (NMR), infrared (IR), ultraviolet–visible (UV/VIS), and mass spectroscopy as well elemental analysis] of this compound are described elsewhere.[5] Polymorphism of this new compound was encountered very late in development. A small change in the last purification step induced the appearance of new polymorphs (Figure 2). At least three different forms (two anhydrous forms, A and B, and a solvated form, C) are thus far known. These forms exhibit unique properties when examined by microscopy, thermal analysis [differential scanning calorimetry (DSC) and thermogravimetric analysis (TG)], IR spectroscopy [solid-state Fourier transform IR (FTIR)], and X-ray powder diffraction (XRPD).

For structure analysis of the solvated form C, single-crystal X-ray diffraction was used. All attempts to synthesize single crystals of the two solvent-free polymorphs A and B that were suitable for single-crystal diffraction failed. Although

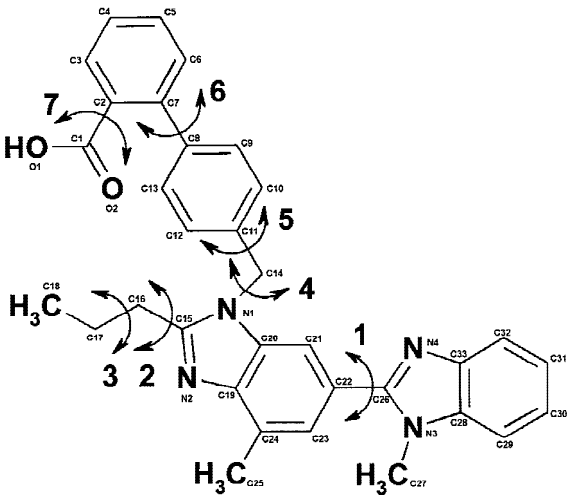

Figure 1. Structural formula of telmisartan (including the numbering scheme of the atoms) with the 7 torsion angles that were varied during the simulated annealing process.

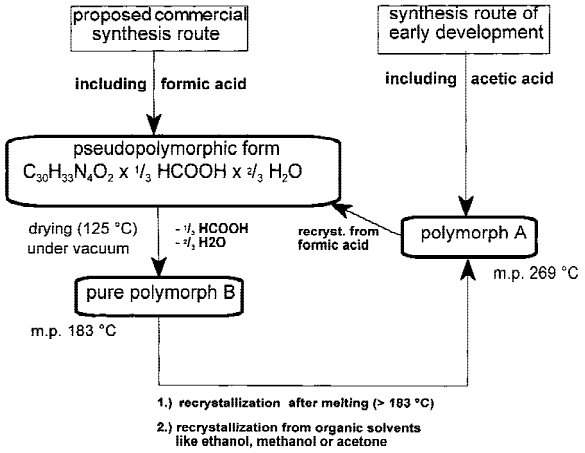

Figure 2. Scheme describing the relationship between the different crystalline modifications of telmisartan.

the morphology of the single crystals of the solvated form C is preserved on drying, the single crystals disintegrate. Therefore, the crystal structures of both of the anhydrous forms A and B were solved by *ab initio* structure determination from high-resolution XRPD patterns by the method of simulated annealing.[6] Polymorph B could not be obtained as single phase, which made successful structure determination from powder data more difficult.

The complexity and accuracy of crystal structure refinements from powder data has been growing steadily since the pioneering work of Hugo Rietveld ~30 years ago.[7] Nowadays, even the crystal structures of small proteins can be refined from high-resolution powder data.[8] On the other hand, it took another 20 years before a considerable number of structure determinations from powder diffraction data appeared in the literature.[9] Most of these early "powder structures" were solved by applying traditional structure-solving methods known from single-crystal analysis to powder data of inorganic solids. With the occurrence of real space methods ~10 years ago, it became possible to determine the crystal structure of molecular compounds. As a prerequisite for the successful application of real space methods, the connectivity within a group of atoms must be known prior to structure determination, which is usually the case for molecules.

The first direct space algorithms were more or less sophisticated grid searches. Random (i.e., Monte Carlo) techniques significantly outperform such grid searches and have allowed structures with ~7 degrees of freedom to be determined.[10–13]

Hence, the latter were used mainly for rigid molecules with few internal degrees of freedom. Simulated annealing was a logical extension of these simple Monte Carlo approaches,[14–18] allowing the crystal structure determination of fairly complex molecular compounds with several internal degrees of freedom (torsion angles) and several molecules in the asymmetric unit.[15–17] Recent advances in this field lie in the treatment of overlapping reflections, the development of faster algorithms, and better annealing schedules.[17] A related approach is to use a genetic algorithm to drive the parameter search.[19,20] Among the various alternative approaches is the minimization of the lattice energy.[21] This method depends strongly on the quality of the potential parameters and the available computing power.

The main focus of this study will be on the structure elucidation by the simulated annealing technique and the consecutive Rietveld analysis from synchrotron XRPD data. This work is one of the first examples in which the previously unknown crystal structures of such a complex compound as telmisartan could be solved from XRPD data by applying a routine procedure.

EXPERIMENTAL SECTION

General Procedures

Material of the higher melting polymorph A of telmisartan was taken from the primary reference standard batch Due 13 (HPLC purity, 99.7%; water content, 0.1%; residual solvents, 40 ppm) without further processing. Large, colorless prismatic crystals of the solvated form C were obtained by recrystallization from 33% formic acid of the higher melting polymorph A. Single crystals of this solvated form are sensitive to drying when removed from the mother liquor. Therefore, for single-crystal X-ray structure analysis, an appropriate crystal was measured with mother liquor in a glass capillary. Material of the lower melting polymorph B was obtained from the solvated form by subsequent drying at 125 °C under vacuum for 2 h.

Microscopy

Photographs of each polymorph were taken with an Olympus BX50 microscope equipped with a video camera. Imaging software analySIS, vers. 2.1, from Soft Imaging System (Muenster, Germany) was used to get printouts of the photographs (Figure 3).

Thermal Analysis

DSC diagrams of each polymorph were recorded with a Mettler DSC 821 at a heating rate of 10

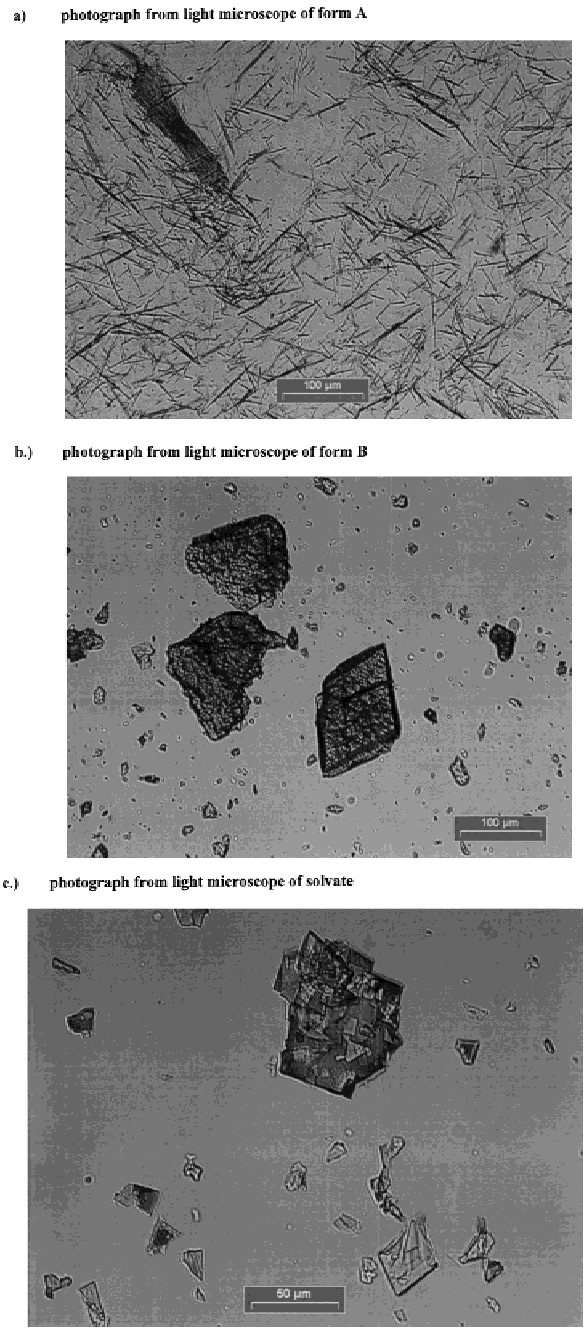

Figure 3. Photographs of the different crystalline forms of telmisartan: (a) form A (long, needle-like crystals); (b) form B (platelet-like crystals with prismatic shape); and (c) solvated form C (platelet-like crystals with prismatic shape).

$K \cdot min^{-1}$ in open Alpans under dry nitrogen atmosphere (Figure 4). Typical sample weights were 5–10 mg. The TG diagrams of each polymorph were recorded with a Mettler Microballance TG 851 at a heating rate of 10 $K \cdot min^{-1}$ in open γ-Al_2O_3 crucibles under dry nitrogen atmosphere. Typical sample weights were 20–30 mg. For data analysis of DSC and TG diagrams, the software package STAR from Mettler Toledo (Giessen, Germany) was used.

FTIR Spectroscopy

Spectra were recorded from KBr disks prepared with each crystal form (1 wt % in KBr) with a Nicolet FTIR spectrometer Magna—IR 560: number of scans, 32; resolution, 4 cm^{-1}; range, 400–4000 cm^{-1} (Figure 5).

X-ray Diffraction Studies

Single-Crystal X-ray Diffraction/Structure Analysis of the Solvated Form

The crystals of the solvated form C of telmisartan are sensitive to drying when removed from the mother liquor. Therefore, a colorless prismatic crystal with approximate dimensions of 0.30 × 0.30 × 0.30 mm was measured with mother liquor in a glass capillary. The use of this preparation technique prevented crystal decay (only 0.7% over timecourse of data collection). All measurements were made on a Rigaku AFC7R diffractometer with graphite monochromated CuK_α radiation and a rotating anode generator at room temperature. Data collection at lower temperatures was not performed.

Neutral atom scattering factors were taken from Cromer and Waber.[22] Anomalous dispersion effects were included in F-calc;[23] the values for $\Delta f'$ and $\Delta f''$ were those of Creagh and McAuley.[24]

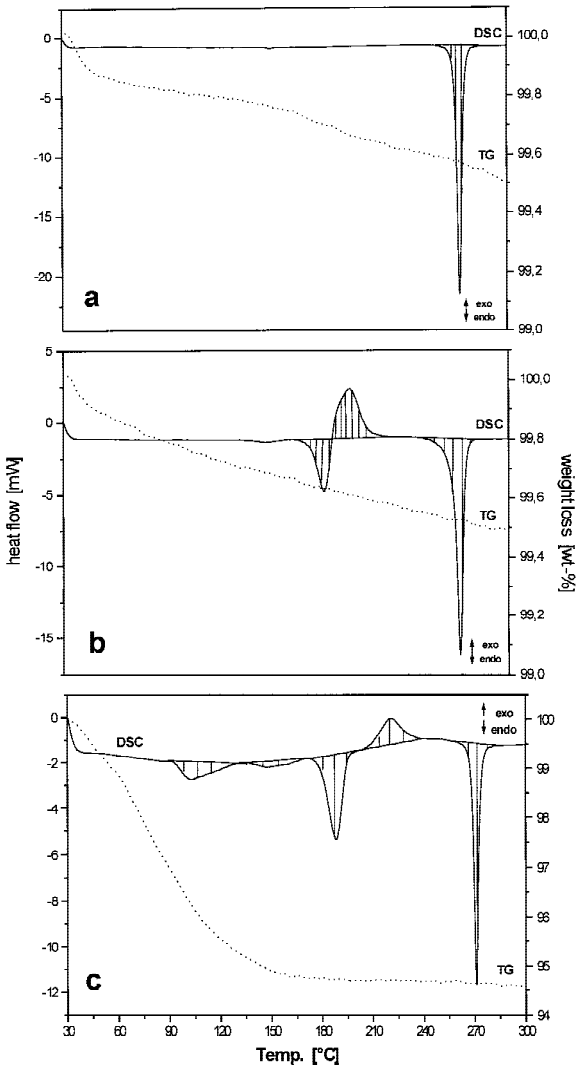

Figure 4. TG/DSC diagrams of the different crystalline forms of telmisartan: (a) form A; (b) form B; and (c) solvated form C.

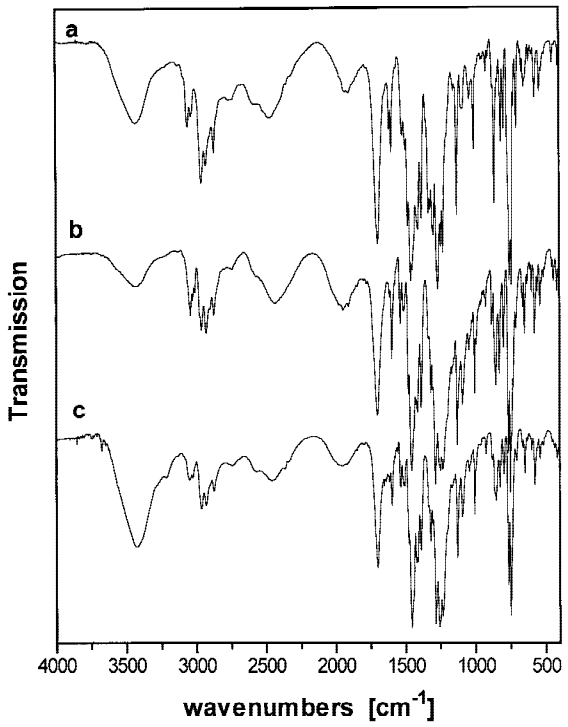

Figure 5. Solid-state IR spectra of the different crystalline forms of telmisartan; (a) form A; (b) form B; and (c) solvated form C.

The values for the mass attenuation coefficients are those of Creagh and Hubbel.[25] All calculations were performed with the teXsan[26] crystallographic software package of Molecular Structure Corporation. Structure solution and refinement was done by direct methods using SHELX.[27] Crystal data are given in Table 1.

A total of 4496 reflections to $\Theta = 55°$ were collected, of which 4397 were unique. The data were corrected for Lorentz and polarization effects. Systematic extinctions suggested space groups *Cc* or *C*2/*c*. The choice of the correct space group *C*2/*c* was based on refinement results. The final cycle of full-matrix least-squares refinement was based on 1989 observed reflections ($F > 4.00\sigma(F)$) and 365 variable parameters and resulted in an agreement factors of $R = 0.135$ ($R = 0.228$, $R_w = 0.379$ for 4169 unique reflections). The maximum and minimum peaks on the final difference Fourier map corresponded to 0.93 and –0.37 $e^-/Å^3$, respectively.

X-ray Powder Diffraction

For the high-resolution XRPD experiments, the samples were sealed in glass capillaries of 0.7-mm diameter (Hilgenberg glass no. 50). Powder diffraction data were collected at room temperature at beamline X3B1 at the National Synchrotron Light Source, Brookhaven National Laboratory (Table 1). The X-ray wavelengths were selected by a double Si(III) monochromator and they were calibrated with the NBS1976 alumina standard. The diffracted beam was analyzed with a Ge(III) crystal and detected with a Na(TI)I scintillation counter with a pulse-height discriminator in the counting chain. The intensity of the primary beam was monitored by an ion chamber. In this parallel-beam geometry, the resolution is determined by the analyzer crystal instead of by slits.[28]

For polymorph A (wavelength 1.14981(2) Å), X-ray scattering intensities were recorded for 2.8 s at each 2Θ in steps of 0.004° from 2.0 to 40.368° (Figure 6a). For polymorph B (wavelength 1.14911(2) Å), X-ray scattering was measured for 2.2 s at each 2Θ in steps of 0.01° from 2.0 to 30.08° (Figure 6b). Samples were spun around Θ during measurement to reduce crystallite size effects.

Both powder patterns are characterized by a rapid fall off of intensity beyond $\sin\Theta/\lambda \approx 0.17$ $Å^{-1}$ (Figure 6). Lowest angle diffraction peaks had a full width at half maximum (fwhm) of 0.018°2Θ for polymorph A and 0.023°2Θ for polymorph B; both of these values are much broader than the resolution of the diffractometer, which is estimated to be <0.008°2Θ for that wavelength. In general, the crystallinity of polymorph A was superior to that of polymorph B. Data reduction was performed using the program GUFI 5.0.[29] Indexing of the powder patterns of polymorphs A and B using the program ITO[30] led to primitive monoclinic unit cells with the lattice parameters given

Table 1. Crystallographic Data for the Crystalline Modifications A, B, and C of Telmisartan

Crystalline Modification	A	B	C
Formula	$C_{33}H_{30}N_4O_2$	$C_{33}H_{30}N_4O_2$	$C_{33}H_{30}N_4O_2$x ⅓ HCOOH × ⅔ H_2O
Temperature [K]	295	295	200
Formula weight [g/mol]	514.63	514.63	541.98
Space group	$P2_1/c$	$P2_1/a$	C2/c
a [Å]	18.7798(3) Å	16.0646(5) Å	30.990(5)
B [Å]	18.1043(2) Å	13.0909(3) Å	13.130(3)
c [Å]	8.00578(7) Å	13.3231(3) Å	16.381(3)
β [Å]	97.066(1)°	99.402(1)°	95.02(2)°
V [$Å^3$]	2701.31 $Å^3$	2764.2(1) $Å^3$	6639(2) $Å^3$
Z	4	4	8
Calc. density [g cm^{-3}]	1.24	1.27	1.08
μ [cm^{-1}]	2.12[a]	2.17[a]	4.90
2Θ range [°]	2.0–40.368	2.0–30.08	—
Step size [°2Θ]	0.004	0.01	—
Counting time/step [s]	2.8	2.2	—
Wavelength [Å]	1.14981(2)	1.14911(2)	1.54178

[a] Calculated for 100% packing in capillary.

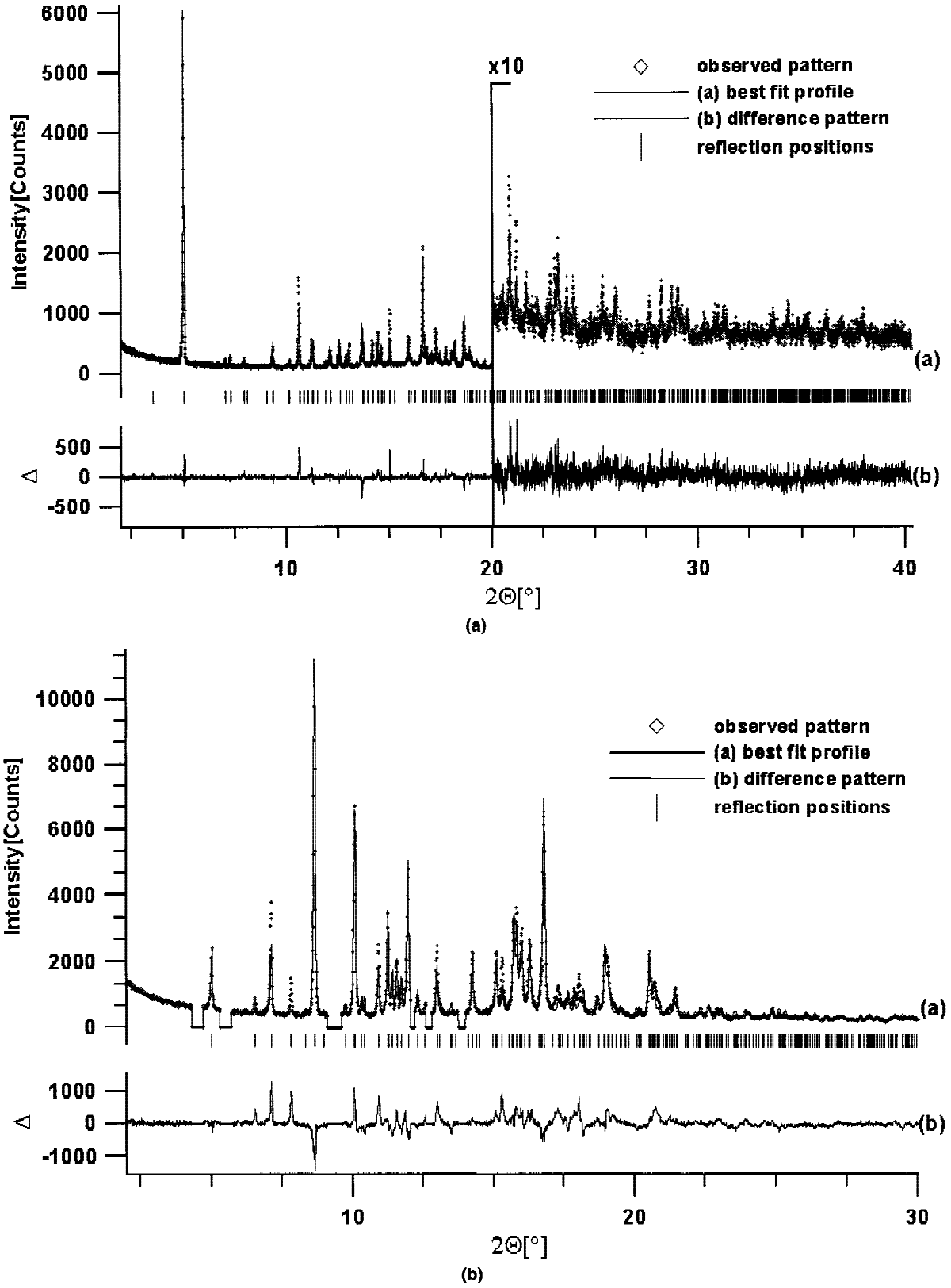

Figure 6. Scattered X-ray intensity for the polymorphic forms A (a) and B (b) of Telmisartan at ambient conditions as a function of diffraction angle 2Θ. Shown are the observed pattern (diamonds), the best Rietveld fit profile (line), the reflection positions, and the difference curve between observed and calculated profile in a different window below. The high angle part of form A is enlarged by a factor of 10 starting at 20° 2Θ. The wavelength was λ = 1.14981(2) Å (form A) and λ = 1.14911(2) Å (form B). The R-values are R-p = 13.4%, R-wp = 17.9% (form A) and R-p = 9.8%, R-wp = 13.0% (form B). R-p and R-wp refer to the Rietveld criteria of fit for profile, and weighted profile respectively, defined in ref. 41.

in Table 1. The space groups could be determined unambiguously as $P2_1/c$ (#14) for polymorph A and as $P2_1/a$ (alternative setting of group #14) for polymorph B from the observed extinction rules. The number of formula units per unit cell could be determined as Z = 4 from packing considerations.

The peak profiles and precise lattice parameters were determined by LeBail-type fits using the program Fullprof.[31] The background was modeled manually using GUFI. The peak profile was described by a pseudo-Voigt in combination with a special function that accounts for the asymmetry due to axial divergence.[32]

A significant amount of an unidentified additional phase (<10%) was observed in several peaks in the powder pattern of polymorph B. This phase, presumably still containing solvent (formic acid, water), is not identical to the formic acid and water-containing phase of the solvated form C, which was previously solved from single-crystal data. It is assumed that the unidentified phase contains less formic acid and water than polymorph C. These solvents could be leftovers of an incomplete drying procedure.

Structure solution of polymorphs A and B was tried by direct methods using the program SIRPOW.[33] All attempts failed, using different sets of starting parameters. This result can be understood in view of massive accidental overlap of peaks, which are typical for a unit cell of that size with low space group symmetry.

Because the connectivity of the atoms was known from a single-crystal study of polymorph C, structure determination for polymorphs A and B was carried out by the simulated annealing technique.[6] For the simulated annealing runs, the program DASH[34] was used. Three input files were needed: a description of the connectivity of the molecules including possible torsion angles, a list of diffraction peak intensities, and a list of parameters to be varied and their ranges for the simulated annealing runs.

For the definition of the connectivity between the atoms within the molecule, we used the Z-matrix notation,[35] which allows for the description of the entire molecule and its intramolecular degrees of freedom by using interatomic distances, angles, and dihedral angles. A flag after each parameter determined whether this parameter was included in the simulated annealing process or not. All intramolecular angles and distances were kept fixed at standard values, allowing only the seven torsion angles to vary (Figure 1).

The diffraction intensities were extracted from a Pawley type refinement, using the program DASH.[34,36] The peak profile was modeled by the Voigt function to which a correction for the asymmetry due to axial divergence was applied. The background was included in the refinement process using high-order Chebyshev polynomials. The covariance matrix of the Pawley fit, which describes the degree of correlation between the individual intensities of neighboring reflections, was actively used in the calculation of the level of agreement between the measured intensities and those of the trial structures after each simulated annealing. It was therefore not necessary to include the entire powder pattern in the simulated annealing procedure, which considerably decreased the computing time needed for each cycle.

The Pawley fit for polymorph A with 260 reflections in the angular range 2–30.0° 2Θ (7001 data points) led to profile values of R_{wp} = 21.14, $R_{expected}$ = 18.15, and χ^2 = 1.36. The Pawley fit for polymorph B with 265 reflections in the angular range 2–30.07° 2Θ (2808 data points) led to profile values of R_{wp} = 18.21, $R_{expected}$ = 9.33, and χ^2 = 3.81. The majority of the misfit can be attributed to the presence of an impurity phase.

A total of 15 parameters was varied during the simulated annealing runs (7 torsion angles, 3 fractional parameters for the position of the molecule, and 4 quaternians[35] describing the orientation of the molecule within the unit cell). The trial structures were generated using a set of numbers chosen randomly in a Monte Carlo fashion within the given range for the 15 parameters.[37]

No special algorithms were employed to prevent close contact of molecules during the global optimization procedure. In general, these have not been found to be necessary because the fit to the structure factors alone quickly moves the molecules to regions of the unit cell where they do not grossly overlap with neighboring molecules.

The crystal structures of forms A and B were fully solved in ~2 h without any use of intervention by the simulated annealing procedure on a personal computer (Pentium II 350 MHz).

For polymorph A, the starting temperature*

* Temperature is not a temperature in thermodynamical sense but refers to the term T in the expression $\exp(\Delta E/KT)$ which is generally known as the Boltzmann factor with the Boltzmann constant K and the state of energy E. The analogous expression with $E = \chi^2_{new} - \chi^2_{old}$ (difference in χ^2 of consecutive cycles) is used as an acceptance criterion in the simulated annealing process.

was determined automatically as 20K with an initial profile χ^2 value for random solution of ~300. After ~3.4 million moves (7000 moves/temperature) in the simulated annealing, the profile χ^2 was 14.3, indicating that the structure was solved. The temperature at this point had fallen to 10.1 K, and the χ^2 for the integrated intensities was 32.8. For polymorph B, the starting temperature was determined automatically as 81 K, with an initial profile χ^2 for random solution of ~100. After ~4.3 million moves in the simulated annealing, the profile χ^2 was 2.91, indicating that the structure was solved. The temperature at this point had fallen to 28.5 K, and the χ^2 for the integrated intensities was 85.4.

In the case of both polymorphs A and B, plotting the χ^2 value of the cost function against iteration number shows the progress made by the simulated annealing algorithm. A long plateau, indicative of a deep local minimum, is evident prior to the final descent into the global minimum (Figure 7).

Once the shift of the parameters went below a predefined minimum, a simplex search was carried out in the surroundings of the parameters to find the absolute minimum.[37]

Final Rietveld refinements were carried out using the program GSAS[38] in which only the scale and overall temperature factors were refined (Figures 6a and 6b). The excellent agreement between the measured and the calculated profile for polymorph A indicates that further refinement might not reveal more structural details. Misfits between the measured and the calculated profile for polymorph B mainly arise from the contamination with an impurity phase, as discussed previously.

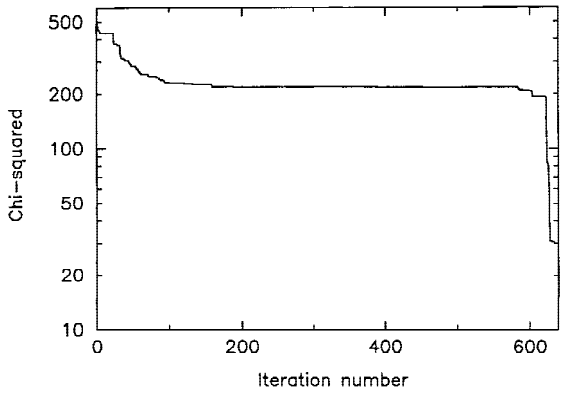

Figure 7. The χ^2 of simulated annealing run of form B in dependence of cycles. The lowest χ^2 value of each cycle is plotted at a time.

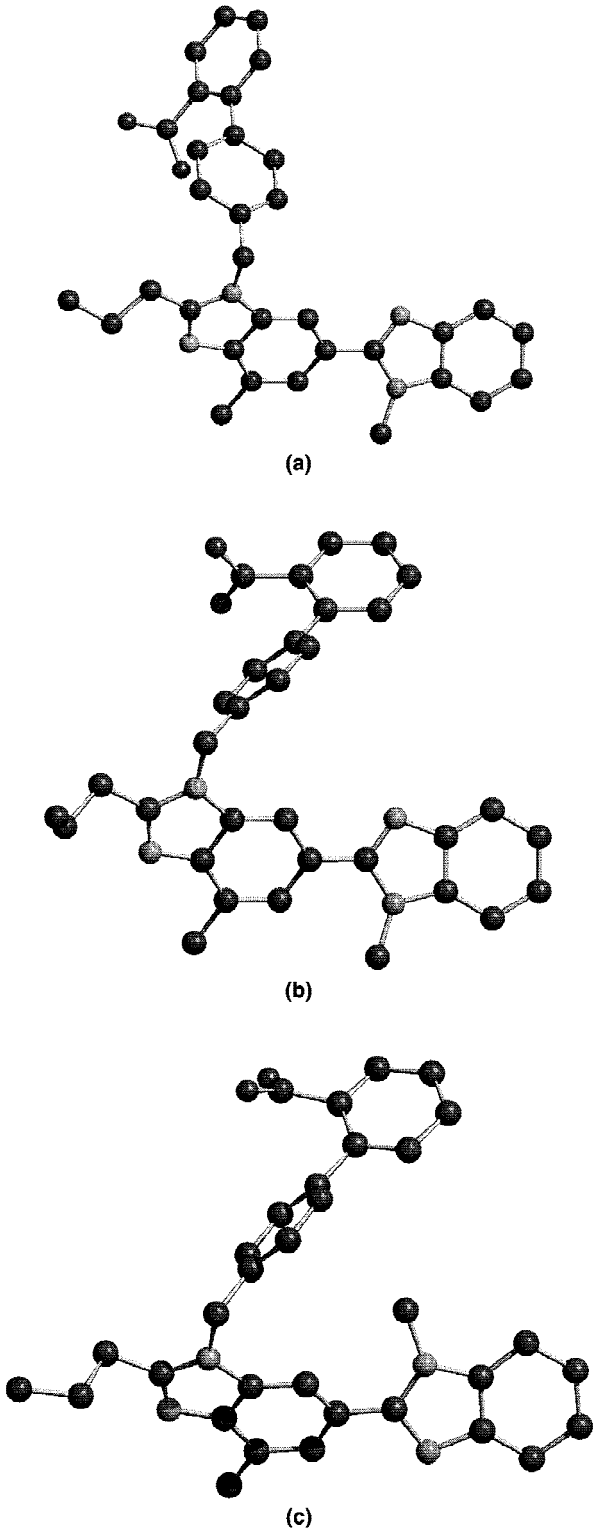

Figure 8. Comparison of molecular conformations of the different crystalline forms of telmisartan (a) form A; (b) form B; and (c) solvated form C.

Table 2. Selected Bond Length [Å] and Torsion Angles [°][a] for the Crystalline Modifications A, B, and C of Telmisartan

Crystalline Modification	No. [b]	A	B	C
N(3)–C(26)–C(22)–C(23)	(1)	–30	–31	149
N(2)–C(15)–C(16)–C(17)	(2)	19	41	84
C(15)–C(16)–C(17)–C(18)	(3)	–169	119	–163
C(20)–N(1)–C(14)–C(11)	(4)	91	52	57
N(1)–C(14)–C(11)–C(10)	(5)	93	42	34
C(13)–C(8)–C(7)–C(6)	(6)	–60	45	46
C(3)–C(2)–C(1)–O(2)	(7)	–37	86	43
Min. intermolecular dist.		O(1)–H–N(4)[c] 2.57	O(1)–H–N(2)[d] 2.54	O(1)–H–N(2)[e] 2.65(5)

[a] The simulated annealing program does not give ESDs of the torsion angles, but they are estimated to be on the order of 5°.
[b] The numbering scheme of the torsion angles refers to Figure 1.
[c] Symmetry transformation: $x, -y + ½, z + ½$.
[d] Symmetry transformation: $-x + ½, y + ½, -z$.
[e] Symmetry transformation: $-x + ½, y + ½, -z + ½$.

The coordinates derived from the simulated annealing runs are presented in Supplementary Materials (Tables S1 and S2) suppl. Material).

RESULTS AND DISCUSSION

General Results

As mentioned in the Introduction, polymorphism of telmisartan was encountered very late in development. The change of the crystalline modification could be traced back to the exchange of acetic acid by formic acid in the last purification step, as indicated in Figure 2. The higher melting polymorph A, consisting of very long needle—like crystals, was obtained from acetic acid (see Figure 3a) with very unfavorable processing properties for production scale synthesis (e.g., extremely hard to filter, very long drying time due to inclusion of solvent, extremely electrostatic, almost no flowing properties of the final powdered material, and with very low tapped density). Telmisartan precipitates in the presence of formic acid in prismatic, platelet-like crystals (see Figure 3b) with much more favorable processing properties than just mentioned. However, as already indicated by the different crystal morphology, this minor variation in the manufacturing procedure results in a change in the crystalline modification of the drug substance. Telmisartan crystallizes in the presence of aqueous formic acid as a solvate with the approximate stoichiometry $C_{33}H_{30}N_4O_2 \times 1/3$ HCOOH $\times$ 2/3 H_2O. Subsequent drying at 125 °C under vacuum leads to the lower melting polymorph B, which crystallizes after melting into the higher melting crystal form A.

The completely different thermal behavior of the polymorphs is also expressed in the DSC diagrams, which are shown in Figure 4. In the DSC diagram of polymorph A, there is only one, single, strong endothermic effect with a maximum at 269 ± 2 °C corresponding to a congruent melting of telmisartan. No significant weight loss is detected in the TG diagram up to 300 °C. Above 300 °C, telmisartan starts to decompose. In addition to the endothermic effect at 269 ± 2 °C, there is another endothermic effect at 183 ± 2 °C immediately followed by an exothermic effect for polymorph B. This thermal behavior is typical for a metastable form of a polymorphic drug substance that has a lower melting point than the stable form and that recrystallizes (= exothermic effect) into the stable form after melting. Also for polymorph B, no significant weight loss is monitored by the TG experiments. The third diagram shown in Figure 4 represents the solvated form C of telmisartan. This diagram has some similarities with the DSC diagram of pure polymorph B, but there are two more small endothermic effects at ~100 and 150 °C in the diagram. These two effects correlate with a weight loss of 5.3% in the TG diagram. About 2.3% of this weight loss is water (from Karl–Fischer titration), and the rest is formic acid [gas chromatography (GC) analysis]. Assuming a possible coprecipitate of telmisartan with formic acid and water in the ratio 3:1:2

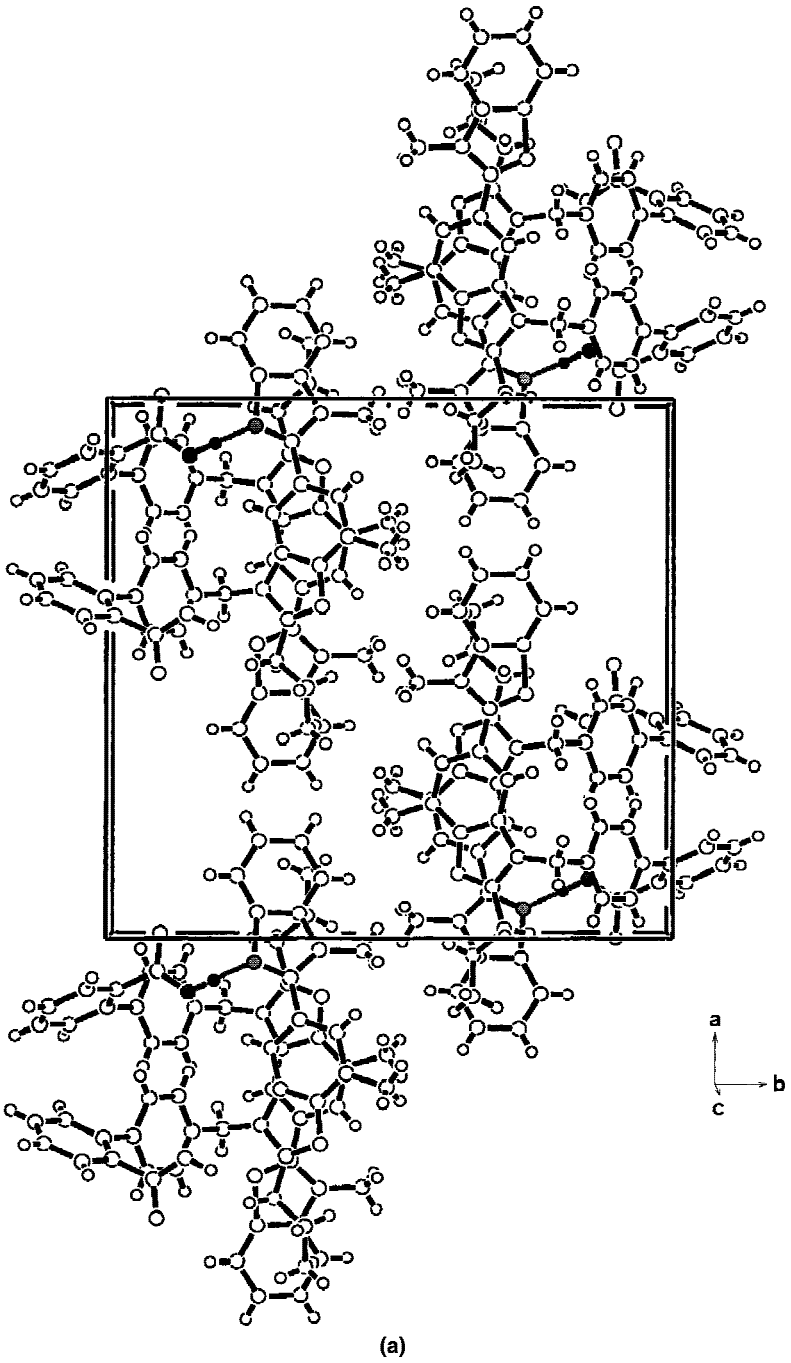

Figure 9. Crystal structure of the anhydrous form A of telmisartan. ORTEP representations of the packing of the molecules: (a) projection along *c* axis (hydrogen bonds are highlighted by colors: red, O atom and bond; blue, H atom; green, N atom); (b) projection along *b* axis (hydrogen bonds cannot be clearly visualized in this projection).

would explain the observed weight loss and the stoichiometry just mentioned.

Solid-state IR spectra revealed significant differences for the polymorphic forms. Figure 5 shows representative examples for the different types of spectra. In the X–H stretching vibration region (2600–3600 cm^{-1} for X = C, N, O) of the two anhydrous crystal forms, the differences in the IR spectra are very small, indicating that the intermolecular binding forces in these two polymorphs are quite similiar. The molecules are held together by hydrogen bonding and/or van der

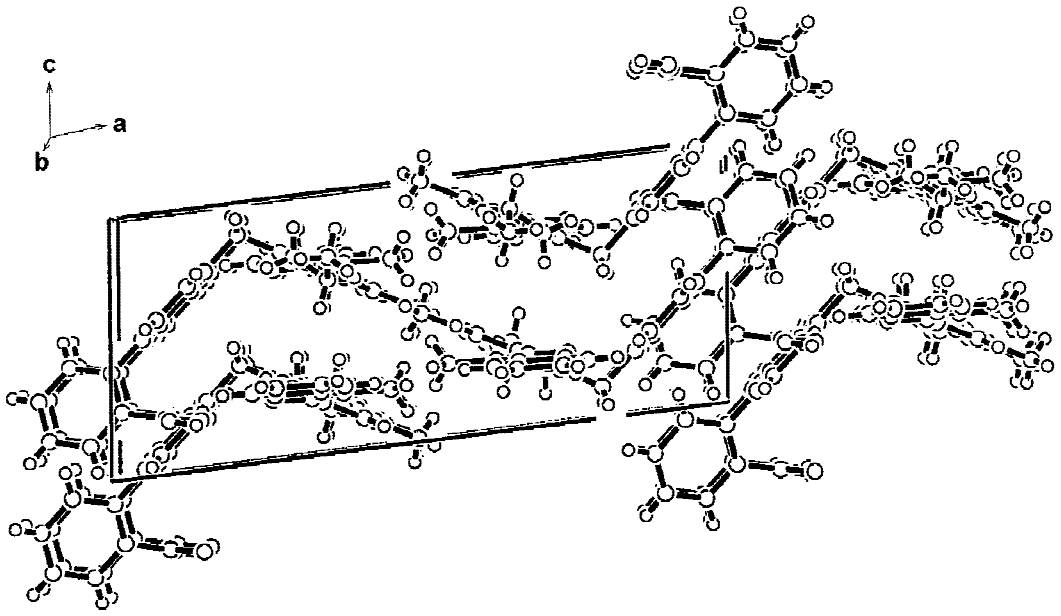

Figure 9. continued.

Waals forces and therefore the X–H stretching vibration region in the IR spectra is most sensitive to such differences. On the other hand, a thorough study of the fingerprint region (400–1800 cm^{-1}) shows significant differences for these two types of spectra. This observation could be interpreted as evidence of differences in the conformation of the telmisartan molecules in these two polymorphs. This phenomenon is known as "conformational polymorphism".[39] This conclusion is nicely confirmed by the X-ray diffraction structure analysis data (vide infra). The IR spectrum of the solvated form C, like the two anhydrous forms, is in the X–H-stretching vibration region. However, in the fingerprint region, significant differences could also be observed.

Crystal Structures

In Figures 8a–c, the molecular conformations of the different crystalline forms of telmisartan are compared. From these figures it is quite obvious that the molecular conformations differ significantly in the three polymorphic forms. In the crystal structure of the anhydrous form A of telmisartan, the characteristic features of the conformation of the molecule is best described as follows (see Figure 8a). The methyl substituent on the terminal benzimidazole group is pointing away from the phenylene moiety as indicated by the torsion angle assigned no. 1 in Figure 1. This positioning results in a more open conformation with an "L-shaped" molecule with an almost rectangular torsion angle no. 4 (see Table 2). In contrast to the structure of form A, the molecules in the solvated form C exhibit a triangular molecular shape in which a close intramolecular contact is realized between the methyl substitutent on the terminal benzimidazole group and the phenylene moiety (see Figure 8c). This conformation may be indicative for a hydrophobic collapse that is probably induced by polar solvents like the formic acid/water medium used here for crystallisation and that is occluded in the crystal structure of form C (vide infra). The characteristic features of the conformation of the molecules of form B (see Figure 8b) are somewhere in between the two extremes represented by forms A and C. The methyl substituent on the terminal benzimidazole group is pointing away from the phenylene moiety as in the anhydrous form A, whereas the overall molecular shape still looks like a triangle, as observed for the solvated form C. These observations are also reflected in the torsion angles assigned 1 and 4 (see Table 2). For forms A and B, torsion angle no. 1 is almost identical, whereas for forms B and C, torsion angle no. 4 is very similar.

The different molecular conformations of the three structures have a strong impact on the packing of the molecules. In Figures 9–11, the crystal structures of the three polymorphic forms are shown from different perspectives with focus

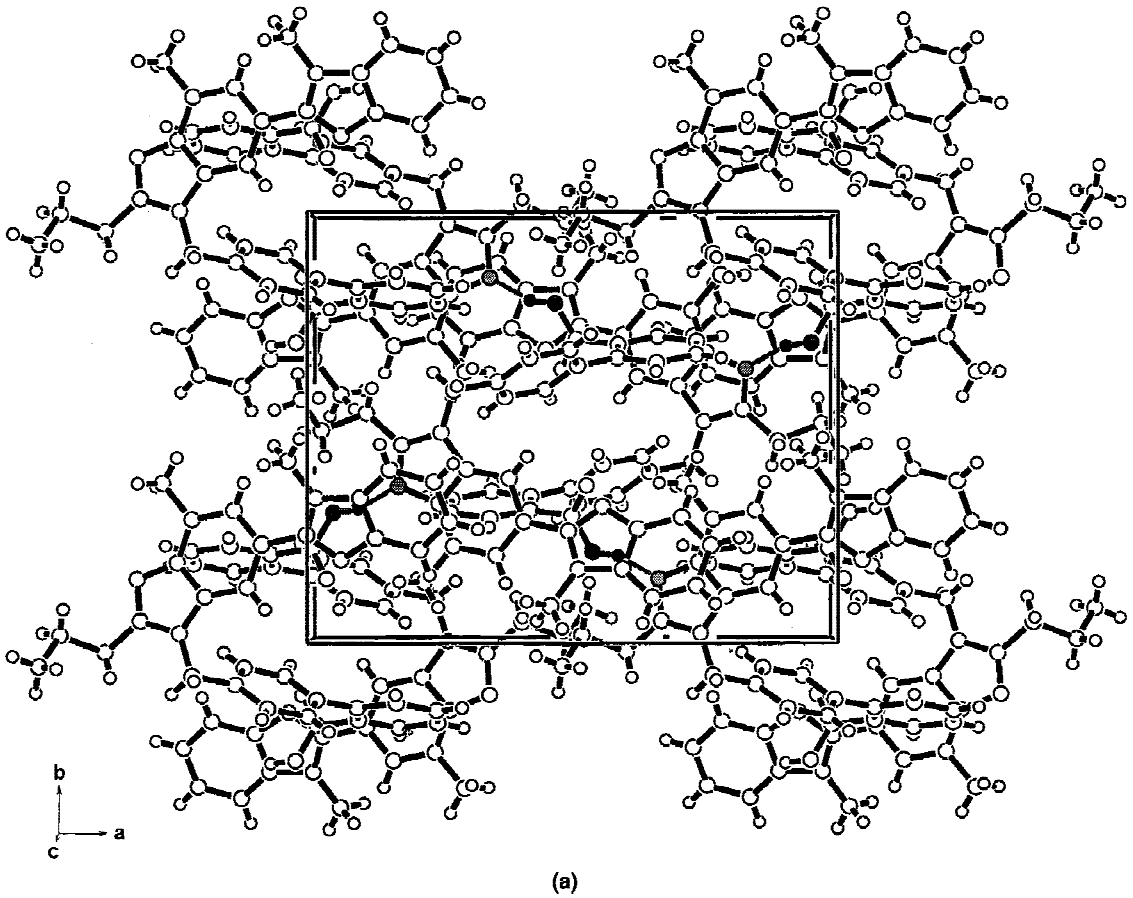

Figure 10. Crystal structure of the anhydrous form B of telmisartan. ORTEP representations of the packing of the molecules: (a) projection along *c* axis (hydrogen bonds are highlighted by colors: red, O atom and bond; blue, H atom; green, N atom); (b) projection along *b* axis (hydrogen bonds cannot be clearly visualized in this projection).

on characteristic packing features of the molecules in the crystal structures.

Before discussing the crystal structures of the three different polymorphs of telmisartan in detail, it should be noted that during data collection on the single crystal of the solvated form C it became apparent that the diffraction intensity dropped unusually fast with increasing resolution so that a significant proportion of the reflections had low intensities. Moreover, the crystallographic refinement converged at the unusually high value of $R = 0.135$. The crystal structure of form C of telmisartan revealed the cause for these findings (see Figure 11). The calculated crystal density is low because of a very porous lattice in which large solvent-filled cavities are interspersed between the telmisartan molecules. The solvent can only partially be modeled with water molecules. No electron density could be interpreted as formic acid, although we know that formic acid is also present in the structure. As a result, the errors in the final structure are relatively high. Nevertheless, the overall molecular structure of form C of telmisartan is unambiguously determined by the present work.

Closer inspection of the crystal packing of form C shows that hydrophobic interactions and a hydrogen bond between the protonated carboxyl oxygen O1 and N2 of the central benzimidazole determine the intermolecular contacts between the drug molecules. A characteristic feature of the crystal structure of form C are large channels along the *c* axis, in which the solvent molecules are mainly disordered (see Figure 11). One water molecule forms a hydrogen bond with N4 on the terminal benzimidazole.

In the structure of form A, the molecules are packed in a completely different way, which results in a more dense structure without cavities or channels with occluded solvent (see Figure 9). The most characteristic features in the packing of the molecules in the crystal structure of form A

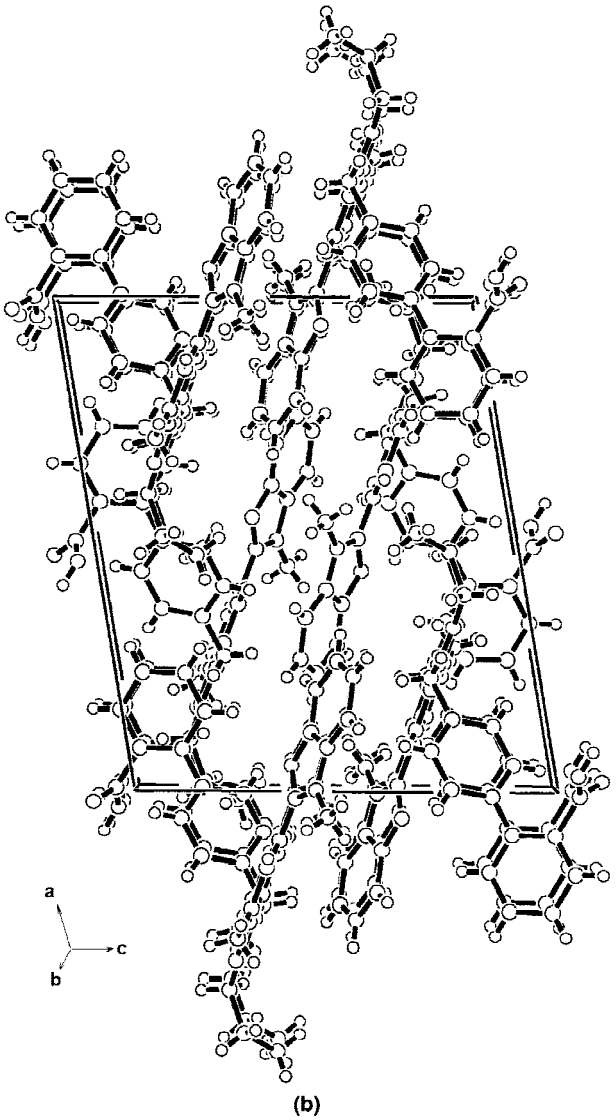

Figure 10. continued.

are the close intermolecular contacts of the methyl and *n*-propyl substituents of the benzimidazole groups (see Figure 9 a), and the parallel stacking (see Figure 9 b) of the central benzimidazole groups (= π–π interaction). Other than these more hydrophobic interactions, there is also a hydrogen bond between the protonated carboxyl oxygen O1 and N4 of the terminal benzimidazole fragment.

The crystal structure of the anhydrous form B of telmisartan, which was obtained by thorough drying of the solvated form C, also displays a condensed molecular packing without cavities or channels (see Figure 10). In this crystal structure, the main hydrophobic interactions are realized by the terminal benzimidazole fragment of one molecule that forms π–π interactions with the central benzimidazole fragment of another molecule on one side and an edge-on aromatic interaction with the phenylene moiety of a third molecule on the other side (see Figure 10). The same intermolecular hydrogen bonding as in the solvated form C also occurs in form B.

It could be shown that moderately complex molecular crystal structures can nowadays be solved quickly and routinely from high resolution XRPD data. The time for structure solution is typically on the order of several hours. Despite these great advances, one has to be aware of the limitations of the powder method that are due to systematic and accidental peak overlap in the powder pattern. It is indisputably possible to determine the molecular conformations with high precision, but it is usually not possible to determine individual bond lengths and angles within the molecules. For this reason, no discussion of bond length and angles of the polymorphs A and B of telmisartan will be included in this paper.

One limitation of the simulated annealing approach (as implemented in DASH), although not of principal nature, is that the algorithm often fails to find the global minimum if there is more than one molecule present in the asymmetric unit. Possible solutions include the use of 'pseudo-atoms' as has been shown for the structure determination of potassiumphenolate[40] with three rigid molecules in the asymmetric unit. A combination of both methods might be powerful enough to allow for the routine determination of even more complicated molecular crystal structures in the near future. Nevertheless, the complexity of most structural problems that occur in pharmaceutical science is comparable to that of the present study.

Acknowledgments

Research was carried out in part at the National Synchrotron Light Source at Brookhaven National Laboratory, which is supported by the US Department of Energy, Division of Materials Sciences and Division of Chemical Sciences. The SUNY X3 beamline at NSLS is supported by the Division of Basic Energy Sciences of the US Department of Energy under Grant No. DE-FG02-86ER45231. Financial support by the Deutsche Forschungsgemeinschaft (DFG) is gratefully acknowledged.

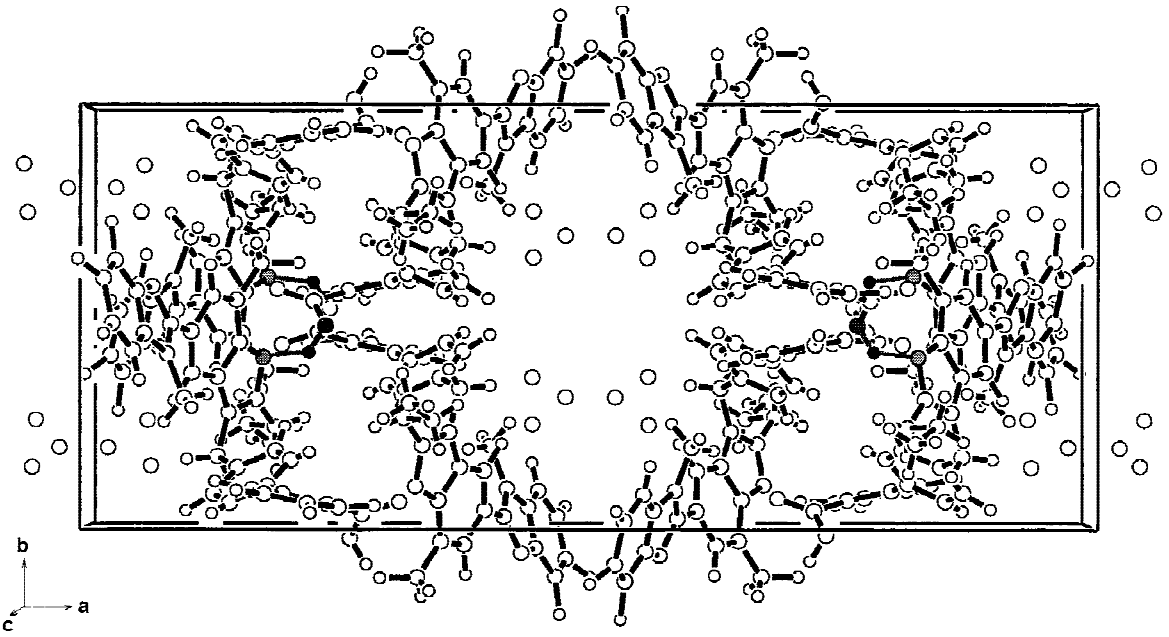

Figure 11. Crystal structure of the solvated form C of telmisartan. ORTEP representations of the packing of the molecules: projection along *c* axis (hydrogen bonds are highlighted by colors: red, O atom and bond; blue, H atom; green, N atom).

REFERENCES

1. Byrn SR. 1982. Solid-State Chemistry of Drugs. New York: Academic Press.
2. Byrn S, Pfeiffer R, Ganey M, Hoiberg C, Poochikian G. 1995. Pharmaceutical solids: A strategic approach to regulatory considerations. Pharm Res 12:945–954.
3. Laragh J. The renin system and the renal regulation of blood pressure. In Seldin DW, Giebisch G, editors. The kidney: Physiology and Pathophiyology, 2nd ed. New York: Raven Press, pp 1411–1453.
4. Hall JE, Brands MW. 1992. The renin-angiotensin-aldosterone system (renal mechanisms and circulatory homeostasis). In Seldin GW, Giebisch G., editors. The Kidney: Physiology and pathophisyology, 2nd ed. New York: Raven Press, pp. 1455–1502.
5. Ries UJ, Miehm G, Narr B, Hasselbach KM, Wittneben H, Entzeroth M, van Meel JCA, Wienen W, Hauel NH. 1993. 6-Substituted benzimidazoles as new nonpeptide angiotensin receptor antagonists: Synthesis, biological activity, and structure-activity relationships. J Med Chem 36:4040–4051.
6. Van Laarhoven PJM, Aarts EHL. 1987. In Simulated annealing: Theory and applications. Dordrecht: D. Reidel Publishing Company.
7. Rietveld HM. 1969. A profile refinement method for nuclear and magnetic structures. J Appl Crystallogr 2:65–71.
8. Von Dreele RB. 1999. Combined Rietveld and stereochemical restraint refinement of a protein crystal structure. J Appl Crystallogr 32:1084–1089.
9. LeBail A. 1999. Structure determination from powder diffraction-Database. http://fluo.univ-lemans.fr:8001/iniref.html, website.
10. Chernyshev VV, Schenk H. 1998. A grid search procedure of positioning a known molecule in an unknown crystal structure with the use of powder diffraction data. Z Krist 213:1–3.
11. Masciocchi N, Moret M, Cairati P, Ragaini F, Sironi A. 1993. Solving simple organometallic structures from X-ray powder diffraction data: The case of polymeric $[\{Ru(CO)_4\}_n]$. J Chem Soc, Dalton Trans 473–475.
12. Bendele GM, Stephens P, Prassides K, Vavekis K, Kordatos K, Tanigaki K. 1998. Effect of charge state on polymeric bonding geometry: The ground state of Na_2RbC_{60}. Phys Rev Lett 80(4):736–739.
13. Dinnebier RE, Stephens PW, Carter JK, Lommen AN, Heiney PA, McGhie AR, Brard L, Smith III AB. 1995. X-ray powder diffraction structure of triclinic $C_{60}Br_{24}(Br_2)_2$. J Appl Crystallogr 28:327–334.
14. Andreev YG, Bruce PG. 1998. Solution of flexible structures from powder diffraction data using a simulated annealing technique. Mat Sci Forum 278–281:14–19.
15. Andreev YG, MacGlashan GS, Bruce PG. 1997. Ab initio solution of a complex crystal structure from powder-diffraction data using simulated-annealing

method and a high degree of molecular flexibility. Phys Rev B 55(18):12011–12017.
16. Andreev YG, Lightfoot P, Bruce PG. 1997. A general Monte Carlo approach to structure solution from powder-diffraction data: Application to poly(ethylene oxide)$_3$:LiN(SO_2CF_3)$_2$. J Appl Crystallogr 30:294–305.
17. David WIF, Shankland K, Shankland N. 1998. Routine determination of molecular crystal structures from powder diffraction data. Chem Commun. 931–932.
18. Newsam JM, Deem MW, Freeman CM. 1992. Direct space methods of structure solution from powder diffraction data. Accuracy in Powder Diffraction II, NIST Spec. Publ. No. 846:80–91.
19. Kariuki BM, Calcagno P, Harris KDM, Philip D, Johnston RL. 1999. Evolving opportunities in structure solution from powder diffraction data—Crystal structure determination of a molecular system with twelve variable torsion angles. Angew Chemie Int Ed 38(6):831–835.
20. Shankland K, David WIF, Csoka T. 1997. Crystal structure determination from powder diffraction data by application of a genetic algorithm. Z Krist 212:550–552.
21. Schmidt MU, Dinnebier RE. 1999. Combination of energy minimizations and rigid body Rietveld refinement: The structure of 2,5-dihydroxybenzo[de]benzo[4,5]-imidazo-[2,1-a]isoquinolin-7-one. J Appl Crystallogr 32:178–186.
22. Cromer DT, Waber JT. 1974. In: International tables for X-ray crystallography, Vol. IV. Birmingham, England: The Kynoch Press. Table 2.2 A.
23. Ibers JA, Hamilton WC. 1964. Dispersion corrections and crystal structure refinements. Acta Crystallogr 17:781–782.
24. Creagh DC, McAuley WJ. 1992. In: Wilson AJC, editor. International Tables for Crystallography, Vol C. Boston: Kluwer Academic Publishers, Table 4.2.6.8, pp 219–222.
25. Creagh DC, Hubbell JH. 1992. In: Wilson AJC, editor. International Tables for Crystallography, Vol C. (A.J.C. Boston: Kluwer Academic Publishers, Table 4.2.4.3, pp 200–206.
26. *teXsan:* Crystal Structure Analysis Package, Molecular Structure Corporation, 1985 & 1992.
27. Sheldrick, G.M. SHELX-97 Manual, University Göttingen.
28. Cox DE. 1991. In: Brown G, Moncton, DeE, editors. Handbook on Synchrotron Radiation, Vol. 3. New York: Elsevier Science Publishers B.V., Chapter 5.
29. Dinnebier RE, Finger LW. 1998. GUFI 5.0. Z Krist Suppl 15:148.
30. Visser JW. 1969. A fully automatic program for finding the unit cell from powder data. J Appl Crystallogr, 89–95.
31. Rodríguez-Carvajal J. 1990. Abstracts of the Satellite Meeting on Powder Diffraction of the Toulouse, France: XV Congress of the IUCr. p. 127.
32. Finger LW, Cox DE, Jephcoat AP. 1994. A correction for powder diffraction peak asymmetry due to axial divergence. J Appl Crystallogr. 27:892–900.
33. Cascarano G, Favia L, Giacovazzo C. 1992. SIRPOW.91 - A direct-methods package optimized for powder data. J Appl Crystallogr 25:310–317.
34. David, WIF. 1999. Simulated annealing program DASH, personal communication.
35. Leach AR. 1996. Molecular Modelling Principles and Applications. Reading, MA: Addison Wesley Longman Limited, pp 2–4.
36. Pawley GS. 1981. Unit-cell refinement from powder diffraction scans. J Appl Crystallogr 14:357.
37. Press WH, Teukolsky SA, Vetterling WT, Flannery BP. 1992. In: Numerical Recipes in Fortran 77, 2nd ed. New York: Cambridge University Press.
38. Larson AC, Von Dreele RB. 1994. GSAS—General Structure Analysis System," Los Alamos National Laboratory Report LAUR 86-748; available by anonymous FTP from mist.lansce.lanl.gov.
39. Stephenson GA, Borchardt TB, Byrn SR, Bowyer J, Bunnell CA, Snorek SV, Yu L. 1995. Conformational and color polymorphism of 5-methyl-2-[(2-nitrophenyl) amino]-3-thiophenecarbonitrile. J Pharm Sci 84:1385–1386.
40. Dinnebier RE, Pink M, Sieler J, Stephens PW. 1997. Novel alkali metal coordination in phenoxides: Powder diffraction results on C_6H_5OM [M = K, Rb, Cs]. Inorg Chem 36:3398–3401.
41. Langford JI, Louër D. 1996. Powder diffraction. Rep Prog Physics 59:131–234.